

Vacuum space-charge effects in nano-ARPESS. Hellmann,^{1,*} T. Ott,² L. Kipp,¹ and K. Rossnagel^{1,†}¹*Institute of Experimental and Applied Physics, University of Kiel, D-24098 Kiel, Germany*²*Institute of Theoretical Physics and Astrophysics, University of Kiel, D-24098 Kiel, Germany*

(Received 21 November 2011; published 7 February 2012)

Angle-resolved photoemission spectroscopy (ARPES) provides a powerful tool for probing the spatially averaged electronic structure of condensed matter at high energy and momentum resolution. Current efforts to add spatial resolution by reducing the focal spot size of the incident radiation to the nanometer regime may result in an effective loss of resolution due to the increased Coulomb interaction between the photoelectrons emitted into vacuum. Here, the potential limitations of “nano-ARPES” at pulsed light sources are determined by molecular-dynamics simulations over a wide range of the most relevant parameters: the pulse duration and focal spot size of the incident light as well as the number of emitted electrons per pulse and their mean kinetic energy. The dependence of the space-charge-induced spectral shift and broadening on these parameters is found to be describable by empirical formulas. The simulation results particularly reveal a saturation of vacuum space-charge effects in the limit of small focal spot sizes and suggest that “nano-ARPES” at an effective energy resolution of 5 meV is possible and practical, employing typical synchrotron radiation in the extreme ultraviolet spectral range.

DOI: [10.1103/PhysRevB.85.075109](https://doi.org/10.1103/PhysRevB.85.075109)

PACS number(s): 79.60.-i, 68.37.Xy, 73.22.-f, 79.77.+g

I. INTRODUCTION

Angle-resolved photoemission spectroscopy (ARPES) is the most direct probe of the occupied part of the electronic structure in solids. The measured data sets typically contain not only the full momentum dependence of the band structure, including the Fermi surface in metallic systems, but also subtle many-body effects that are reflected in the widths and shapes of the spectral lines as well as in gaps, kinks, and other modifications of the band dispersion on the meV energy scale.¹⁻³ ARPES has played a key role in clarifying the electronic properties of cuprate-based high-temperature superconductors⁴ and is presently one of the most important techniques to study frontier materials such as graphene,⁵ topological insulators,⁶ or iron-based high-temperature superconductors.⁷ For the most part, this success story rests on the parallel development of high-resolution electron spectrometers with highly parallel detection^{8,9} and high-brilliance extreme ultraviolet and soft x-ray beamlines at third-generation synchrotron-radiation sources.

In the standard approach, ARPES is a temporally and spatially integrating technique. Yet, two current trends seek to overcome these limitations. One is to add femtosecond time resolution in order to be able to probe the dynamics of electronic structure at the natural time scales of electronic and structural processes. Femtosecond ARPES has recently been realized in the ultraviolet^{10,11} and extreme ultraviolet¹² regime using table-top laser systems plus fourth-harmonic¹³ and higher-harmonic¹⁴ generation. The other trend is to focus the incident light to ever-smaller dimensions, ultimately to nanometer length scales, which would allow us to study the electronic structure of individual nanometer-sized samples or sample domains. Employing optical elements such as ellipsoidal mirrors, Schwarzschild objectives, Fresnel zone plates, or photon sieves,^{15,16} some progress toward photoemission microspectroscopy has recently been made,^{17,18} mostly in chemical imaging of elementally segregated surfaces.¹⁹⁻²¹ However, true nanometer ARPES (“nano-ARPES”) at the high

energy and angle resolutions achieved in the standard approach has not yet been realized.

Both ARPES trends rely on the use of pulsed light sources. While femtosecond ARPES naturally requires femtosecond pulse durations, the prospects of nanometer ARPES seem best when the highly stable undulator radiation at third-generation sources with typical pulse durations of a few 10 ps is used. The use of short-pulsed radiation in solid-state photoemission, however, implies a potentially strong limitation: Each photon pulse may lead to the emission of a dense cloud of photoelectrons from the surface and the mutual Coulomb repulsion between the electrons may severely distort the initial energy and angular distribution on the passage to the detector, thus leading to an effective loss of energy and momentum resolution. In reality, vacuum space charge has been shown to cause spectral shifts and broadenings of up to 10 meV in photoemission experiments at third-generation synchrotron radiation sources²² and of several eV at free-electron lasers and ultrafast optical laser systems.^{23,24}

To describe the experimentally observed effects, simple analytical models as well as *ab initio* numerical simulations have successfully been used. In particular, it has been possible to establish simple functional dependencies on the key parameters, i.e., the number of emitted photoelectrons, the focal spot size on the surface, the photon pulse duration, and the photoelectron kinetic energy distribution.²⁴⁻²⁸ The aim of the present work is to extend our earlier study²⁷ to specifically explore the limits of nano-ARPES due to vacuum space charge. The focus thus lies on the influence of the focal spot width as it is decreased to nanometer length scales. As in our previous work,²⁷ we use a completely general *ab initio* approach on the basis of a *N*-body molecular dynamics model to simulate the electron propagation from the surface to the detector. Our main finding is the saturation of vacuum space-charge effects in the limit of small focal spot sizes, which implies that nano-ARPES with sub-100-nm spatial resolution and 5 meV effective energy resolution is not only possible but also practical when typical

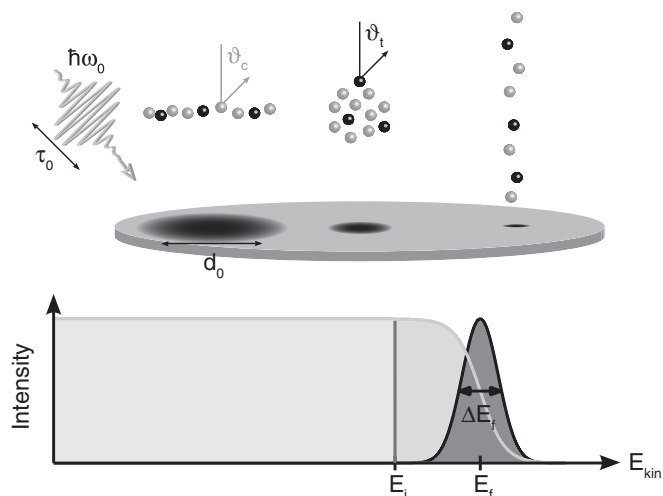


FIG. 1. Schematic of photoemission from a solid surface using monochromatic light pulses with an energy $\hbar\omega_0$, a duration τ_0 , and a focal width d_0 . With decreasing ratio d_0/τ_0 , the shape of the emitted electron cloud changes from a quasi-2D disk via a 3D sphere to a quasi-1D chain. Within the numerical simulation, the emitted electrons are divided into cloud electrons (gray dots) and test electrons (black dots), both having specified initial kinetic energy and emission angle ($\vartheta_{c,i}$) distributions. In all simulations presented in this work, the test electrons start with a fixed energy E_i , while the cloud electrons are uniformly distributed over the energy interval $[0, E_i]$ (light gray filling). After each simulation run, the space-charge-induced spectral shift and broadening are obtained by fitting a Gaussian to the final test electron energy distribution (dark gray filling). The shift and broadening are defined as the Gaussian mean energy shift $E_f - E_i$ and the Gaussian full width at half maximum ΔE_f , respectively.

undulator radiation is used. For the practitioner we condense the results of our simulations into simple empirical formulas.

II. COMPUTATIONAL MODEL

Since our numerical simulation model is described in detail in Ref. 27, we only give a brief description here. Figure 1 shows a sketch of solid-state photoemission using a pulsed light source: A monochromatic photon pulse of energy $\hbar\omega_0$ and duration τ_0 causes emission of photoelectrons from a surface area with a characteristic width d_0 . The initial shape of the photoelectron cloud should strongly depend on the ratio $d_0/(\tau_0 \sqrt{2E_i/m_e})$, where E_i denotes the initial maximum kinetic energy and m_e the electron mass. The three principal shapes of the electron cloud are illustrated in Fig. 1: a quasi-two-dimensional disk, a three-dimensional sphere, and a quasi-one-dimensional chain, corresponding to situations in which $d_0/(\tau_0 \sqrt{2E_i/m_e}) \gg 1$, ≈ 1 , and $\ll 1$, respectively.

In the beginning of the simulation, the cloud, which in the end will contain N_c electrons, is gradually built up assuming Gaussian temporal and spatial profiles with full widths at half maxima of τ_0 and d_0 , respectively. The simulation is propagated in time by numerical integration according to the leap-frog method. The Coulomb force is calculated via the hierarchical tree-code scheme requiring only $O(N_c \log N_c)$ operations.²⁹ The simulation is typically terminated after a propagation time of a few nanoseconds, when the Coulomb

force on the electrons in the cloud becomes negligible and the electrons travel ballistically toward the detector. The final kinetic energy distribution of the electrons is then calculated as it would appear in the detector. This procedure is repeated ten times for each parameter set to obtain some statistics and an error estimate.

In real ARPES experiments, the photoelectrons are emitted into the entire hemisphere above the surface and their kinetic energy distribution is typically broad. Thus, at high energy and angle resolution, only a marginal number of the electrons reaches the detector. To increase the efficiency and statistical significance of the simulation, we have introduced so-called test electrons, with kinetic energy and emission angle distributions specified such that the trajectories always end in the detector. The test electrons feel the Coulomb force of the cloud electrons but they do not contribute to this force.

In ARPES, the feature of highest interest—the Fermi edge—sits on top of a background that contains most of the emitted electrons. To model this condition, a rectangular energy distribution of the cloud electrons extending from 0 to E_i , the fixed initial energy of the test electrons, is assumed (Fig. 1). At the end of the simulation, the leading edge of the energy distribution of the cloud electrons will be broadened and shifted to higher energies and the initial Dirac-like spectrum of the test electrons will be broadened and shifted in a similar way. The space-charge-induced spectral shift and broadening are quantified by fitting a Gaussian to the final test electron spectrum (see Fig. 1).

We note that the angular distribution of the emitted electrons will be smeared by vacuum space charge as well. However, compared to the spectral distortions, this effect is known to be small²⁷ and will not be considered here. The focus of the present work is the dependence of the space-charge-induced spectral shifts and broadenings on the key parameters: N_c , d_0 , τ_0 , and E_i .

III. RESULTS AND DISCUSSION

Figure 2 displays the numerically simulated energy shift and broadening as a function of the focal spot diameter d_0 for $N_c = 1000$, $E_i = 50$ eV, and two pulse durations of $\tau_0 = 20$ ps and $\tau_0 = 100$ ps, i.e., for typical parameters of an ARPES experiment at a third-generation synchrotron radiation source. The spot diameter is varied between 1 mm and 1 nm and thus covers standard ARPES as well as nano-ARPES conditions. Note, however, that the lowest spot widths in this range are idealistic as the Rayleigh resolution of a Fresnel zone plate or other diffractive or reflective optical elements is limited to ~ 14 nm at a photon energy of $\hbar\omega_0 = 55$ eV (assuming a typical work function of $W = 5$ eV; $E_i = \hbar\omega_0 - W$).

Figure 2 directly reflects the dimensional crossover in the shape of the electron cloud upon changing d_0 . In our previous study²⁷ we found that for large spot diameters vacuum space-charge effects are independent of the pulse duration and solely proportional to the initial electron density N_c/d_0 . The results in Fig. 2 show that for pulse durations of several 10 ps, the underlying assumption of a disk-shaped electron cloud already becomes invalid for spot diameters smaller than about 100 μm , as the data points for the two different pulse durations start to separate around this value. The regime of a spherical

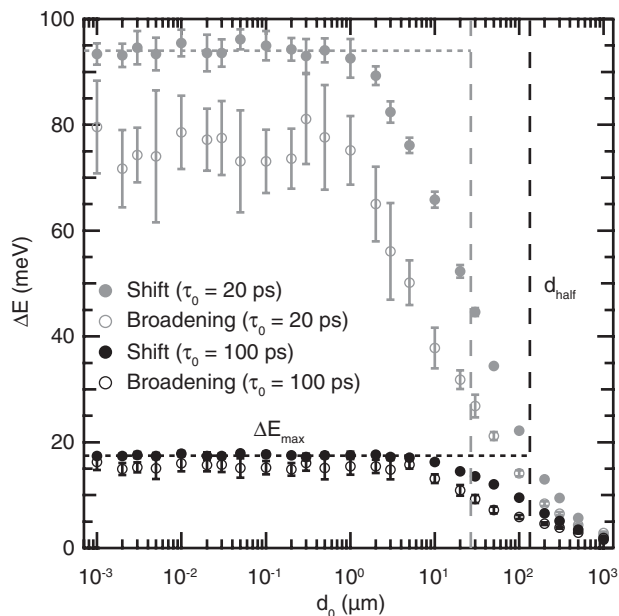


FIG. 2. Simulated space-charge-induced energy shift and broadening as a function of the spot diameter d_0 for a typical ARPES experiment. The error bars represent the standard deviations of repeated simulations. Data for pulse durations of 20 and 100 ps are shown. In the simulations, the test electrons have an initial kinetic energy $E_i = 50$ eV and sit on top of a uniform distribution of cloud electron energies in the interval $[0, E_i]$. The number of cloud electrons is $N_c = 1000$. The cloud electrons are emitted isotropically over the hemisphere, whereas the test electrons are emitted in the surface normal direction. The dashed horizontal and vertical lines mark plateau energies (ΔE_{\max}) in the quasi-1D regime and the half-way spot diameter (d_{half}) between the quasi-1D and quasi-2D regimes, respectively.

electron cloud is entered and the space-charge-induced shift and broadening depend on both the spot diameter and the pulse duration. Indeed, for the chosen parameters, this dimensional crossover is expected to occur around $d_0 = \sqrt{2E_i/m_e}\tau_0 \approx 80\text{--}420$ μm . Then, for $d_0 \lesssim 1$ μm , the space-charge effects

become independent of the spot diameter as they saturate at maximum energies ΔE_{\max} that depend strongly on the pulse duration (dashed horizontal lines in Fig. 2). This behavior is consistent with the emission of a chain-like electron cloud whose (linear) density is proportional to $N_c/(\tau_0\sqrt{E_i})$ rather than to N_c/d_0 .

Figure 3 reveals the functional dependence of the plateau energies ΔE_{\max} on the pulse duration τ_0 [Fig. 3(a)], the kinetic energy E_i [Fig. 3(b)], and the number of electrons per pulse N_c [Fig. 3(c)]. The underlying simulations were performed with the same energy and angular distributions as used for Fig. 2, but at a fixed spot size of $d_0 = 10$ nm. The other parameters were either held fixed ($\tau_0 = 50$ ps, $E_i = 50$ eV, $N_c = 1000$) or varied according to the horizontal axis of the graphs.

In the quasi-1D regime, as noted above, it is reasonable to expect that vacuum space-charge effects depend on the initial electron density $N_c/(\sqrt{2E_i/m_e}\tau_0)$, where the denominator gives the spread of the electron cloud in the direction perpendicular to the surface. In fact, the corresponding power law dependencies on the three parameters— τ_0 , E_i , and N_c —reproduce the numerically simulated results plotted in Figs. 3(a)–3(c) almost perfectly. From fits of the equation

$$\Delta E_{\max}^{S,B} = \theta^{S,B} \cdot \frac{N_c}{\sqrt{E_i}\tau_0} \quad (1)$$

to the simulated energy shifts and broadenings, we determine the scaling factors for the shift and broadening to be $\theta^S = 13.2 \pm 0.3$ and $\theta^B = 10.7 \pm 0.3$ ($\Delta E_{\max}^{S,B}$ in meV, E_i in eV, τ_0 in ps). However, we emphasize that these values depend strongly on the form of the photoelectron energy and angular distributions and the possible inclusion of mirror-charge effects.²⁷

The d_0 dependence of the spectral shift and broadening as displayed in Fig. 2 shows that not only the plateau energies $\Delta E_{\max}^{S,B}$ in the quasi-1D regime are a function of the parameter τ_0 , but also the spot diameters $d_{\text{half}}^{S,B}$ at which the quasi-1D behavior sets in (dashed vertical lines). We define $d_{\text{half}}^{S,B}$ as the

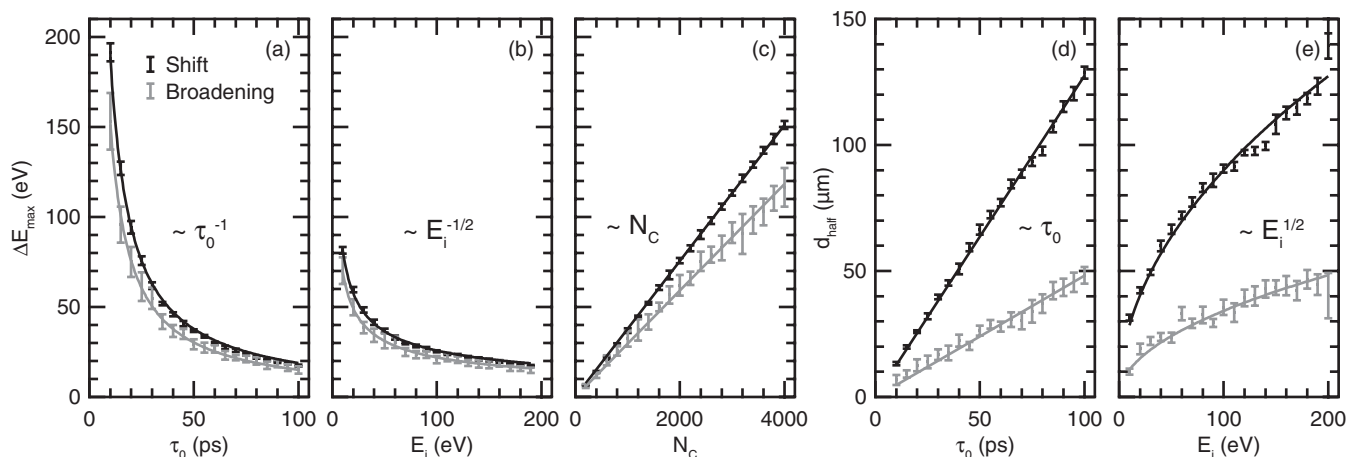


FIG. 3. Vacuum space-charge effects in the small spot diameter limit ($d_0 = 10$ nm). (a)–(c) Maximum energy shift and broadening ΔE_{\max} as a function (a) of the pulse duration τ_0 ($E_i = 50$ eV, $N_c = 1000$), (b) of the kinetic energy E_i ($\tau_0 = 50$ ps, $N_c = 1000$), and (c) of the number of electrons per pulse N_c ($\tau_0 = 50$ ps, $E_i = 50$ eV). (d), (e) Half-way spot diameter d_{half} as a function (d) of τ_0 ($E_i = 50$ eV) and (e) of E_i ($\tau_0 = 50$ ps) (in both cases: $N_c = 5\sqrt{E_i}\tau_0$ eV $^{-1/2}$ ps $^{-1}$). Solid lines represent power-law fits as indicated.

d_0 values where the energy shift and broadening are equal to $\Delta E_{\max}^{S,B}/2$. It seems evident that $d_{\text{half}}^{S,B}$ should also depend on the parameter E_i . Figures 3(d) and 3(e) show $d_{\text{half}}^{S,B}$ as a function of τ_0 and E_i , respectively. The plotted $d_{\text{half}}^{S,B}$ values were interpolated from spectral shifts and broadenings that were simulated as a function of the spot diameter for varying values of the pulse duration and the kinetic energy at a constant fraction $N_c/(\sqrt{E_i}\tau_0) = 5 \text{ eV}^{-1/2}\text{ps}^{-1}$. The critical spot sizes $d_{\text{half}}^{S,B}$, which basically mark the transition between disk-like and chain-like electron clouds, have to be of the order $\tau_0\sqrt{2E_i/m_e}$, i.e., the initial extension of the electron cloud in the direction of the surface normal. It is, therefore, not surprising that the respective linear and square-root dependencies on the parameters τ_0 and E_i describe the data in Figs. 3(d) and 3(e) very well.

Our goal now is to derive an empirical formula that describes the space-charge-induced spectral shift and broadening over the full range of focal spot widths. Since the quasi-1D and quasi-2D regimes can both be represented by 1D electron densities [$N_c/(\sqrt{2E_i/m_e}\tau_0)$ and N_c/d_0 , respectively], our ansatz is to simply take the quadratic mean of the two:

$$\Delta E^{S,B} = \theta^{S,B} \cdot \frac{N_c}{\sqrt{\xi^{S,B}d_0^2 + E_i\tau_0^2}}. \quad (2)$$

The dimensional scaling factors for the shift and broadening, $\xi^{S,B}$, can be determined from the fits depicted in Figs. 3(d) and 3(e) and the relation $\xi^{S,B} = 3E_i(\tau_0/d_{\text{half}}^{S,B})^2$. The best-fit values are $\xi^S = 93 \pm 3$ and $\xi^B = 640 \pm 20$ ($\Delta E_{\max}^{S,B}$ in meV, d_0 in μm , E_i in eV, τ_0 in ps).

Figure 4 compares the predictions of Eq. (2) to the results of molecular-dynamics simulations over a wide spot diameter interval ranging from 1 nm to 1 mm. The simulations were performed for pulse durations τ_0 and kinetic energies E_i varying between 10 and 200 eV and 10 and 100 ps, respectively, at a constant fraction $N_c/(\sqrt{E_i}\tau_0) = 5 \text{ eV}^{-1/2}\text{ps}^{-1}$. The resulting average values and maximum deviations are indicated in Fig. 4 together with the average values given by Eq. (2) for the same parameter sets.

The overall agreement between the empirically predicted and numerically simulated results is good. In the plateau region ($d_0 < 1 \mu\text{m}$), the agreement is excellent implying the validity of Eq. (1). The poorer agreement in the transition region (specifically for $d_0 > 50 \mu\text{m}$) can be traced back to the dimensionality crossover and the associated change in the coordination number: In the quasi-1D regime an electron has two nearest neighbors; in the quasi-2D regime the coordination number is about 6; and in the 3D regime in-between it is about 10. Since vacuum space-charge effects depend on both the nearest-neighbor distance and the number of nearest neighbors and since the increase of the coordination number in the transition region is not included in the empirical model, it is not surprising that Eq. (2) can underestimate the space-charge effects in this region by a factor of 3–5.

Equation (2) seems to provide a robust estimate of the magnitude of the spectral deterioration to be expected in ARPES experiments. Unfortunately, corresponding experimental data are scarce. An exception is a laser-based spectromicroscopy experiment³⁰ that was performed in the quasi-1D regime

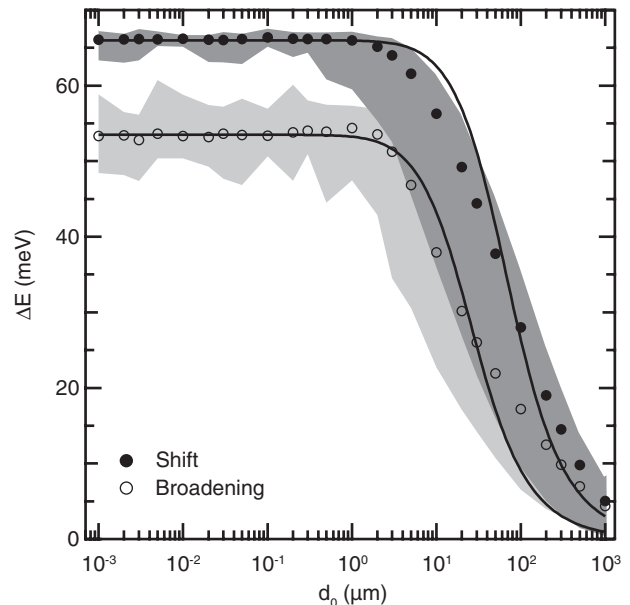


FIG. 4. Simulated space-charge-induced energy shift and broadening (filled and open circles) as a function of the spot diameter d_0 in comparison to values calculated by formula (2) (solid lines). The circles and lines represent average values for the following parameter ranges: kinetic energy $E_i \in [10, 200]$ eV, pulse duration $\tau_0 \in [10, 100]$ ps, and number of electrons per pulse $N_c = 5\sqrt{E_i}\tau_0 \text{ eV}^{-1/2}\text{ps}^{-1}$. The gray shaded areas indicate the maximum variation of the numerically simulated results.

characteristic of nano-ARPES. For the parameters of the experiment ($N_c = 5 \cdot 10^5$, $d_0 = 3.5 \mu\text{m}$, $\tau_0 = 5 \text{ ns}$, $E_i = 6 \text{ eV}$), Eq. (2) predicts an energy broadening of about 440 meV, whereas the experimentally observed broadening was about 200 meV. This rough agreement is remarkable, given that the experimental pulse duration of 5 ns is larger by a factor of 50 than the maximum pulse duration considered in our numerical simulations.

IV. CONCLUSION

Vacuum space charge sets a fundamental limit to the achievable energy resolution in solid-state photoemission at pulsed high-brilliance photon sources. To determine the role of vacuum space-charge effects in future nano-ARPES experiments, we have performed molecular dynamics simulations in the relevant region of the parameter space spanned by the key parameters: the focal width and the pulse duration of the incident light and the number and kinetic energy of the emitted electrons. Our results show that vacuum space-charge dynamics is largely determined by the initial shape of the electron cloud and that the space-charge-induced spectral shift and broadening can be approximated by simple empirical formulas.

The most important conclusion of our study is that nano-ARPES is a viable technique because, upon decreasing the focal spot width to below $1 \mu\text{m}$, the space-charge-induced spectral shift and broadening saturate at moderate values that only depend on the number of emitted electrons per pulse, their kinetic energy, and the pulse duration. Using the empirical formulas derived in this work, we can estimate the efficiency

of the technique. If an effective energy resolution of 5 meV is wished for at 25-nm spatial resolution, the number of emitted electrons per pulse has to be kept below about 165 (assuming an electron kinetic energy of 50 eV and a photon pulse duration of 50 ps). This is only a factor of about six lower than the roughly 1000 photoelectrons emitted per pulse

in spatially averaging high-resolution ARPES experiments at third-generation synchrotron radiation sources.²² However, since this factor could in principle be compensated for by combining more efficient electron detection schemes³¹ with high-speed³² 2D detectors, nano-ARPES measurements not only seem possible but also practical.

*hellmann@physik.uni-kiel.de

†rossnagel@physik.uni-kiel.de

¹S. D. Kevan, *Angle-Resolved Photoemission: Theory and Current Applications* (Elsevier, Amsterdam, 1992).

²S. Hüfner, *Photoelectron Spectroscopy—Principles and Applications* (Springer, Berlin, 2003).

³W. Schattke and M. A. Van Hove, *Solid State Photoemission and Related Methods—Theory and Experiment* (Wiley-VCH, Weinheim, 2003).

⁴A. Damascelli, Z. Hussain, and Z.-X. Shen, *Rev. Mod. Phys.* **75**, 473 (2003).

⁵T. Ohta, A. Bostwick, T. Seyller, K. Horn, and E. Rotenberg, *Science* **313**, 951 (2006).

⁶M. Z. Hasan and C. L. Kane, *Rev. Mod. Phys.* **82**, 3045 (2010).

⁷D. H. Lu, M. Yi, S.-K. Mo, A. S. Erickson, J. Analytis, J.-H. Chu, D. J. Singh, Z. Hussain, T. H. Geballe, I. R. Fisher, and Z.-X. Shen, *Nature (London)* **455**, 81 (2008).

⁸N. Mårtensson, P. Baltzer, P. A. Brühwiler, J.-O. Forsell, A. Nilsson, A. Stenborg, and B. Wannberg, *J. Electron Spectrosc. Relat. Phenom.* **70**, 117 (1994).

⁹B. Wannberg, *Nucl. Instrum. Meth. Phys. Res. A* **601**, 182 (2009).

¹⁰L. Perfetti, P. A. Loukakos, M. Lisowski, U. Bovensiepen, H. Berger, S. Biermann, P. S. Cornaglia, A. Georges, and M. Wolf, *Phys. Rev. Lett.* **97**, 067402 (2006).

¹¹F. Schmitt, P. S. Kirchmann, U. Bovensiepen, R. G. Moore, L. Rettig, M. Krenz, J.-H. Chu, N. Ru, L. Perfetti, D. H. Lu, M. Wolf, I. R. Fisher, and Z.-X. Shen, *Science* **321**, 1649 (2008).

¹²T. Rohwer, S. Hellmann, M. Wiesenmayer, C. Sohr, A. Stange, B. Slomski, A. Carr, Y. Liu, L. M. Avila, M. Källäne, S. Mathias, L. Kipp, K. Rossnagel, and M. Bauer, *Nature (London)* **471**, 490 (2011).

¹³F. Rotermund and V. Petrov, *Opt. Lett.* **23**, 1040 (1998).

¹⁴R. Haight and D. R. Peale, *Rev. Sci. Instrum.* **65**, 1853 (1994).

¹⁵D. Attwood, *Soft X-Rays and Extreme Ultraviolet Radiation—Principles and Applications* (Cambridge University Press, Cambridge, 1999).

¹⁶L. Kipp, M. Skibowski, R. L. Johnson, R. Berndt, R. Adelung, S. Harm, and R. Seemann, *Nature (London)* **414**, 184 (2001).

¹⁷A. Barinov, P. Dudin, L. Gregoratti, A. Locatelli, T. O. Menten, M. A. Nino, and M. Kiskinova, *Nucl. Instrum. Meth. Phys. Res. A* **601**, 195 (2009).

¹⁸M. Källäne, J. Buck, S. Harm, R. Seemann, K. Rossnagel, and L. Kipp, *Opt. Lett.* **36**, 2405 (2011).

¹⁹U. Johansson, R. Nyholm, C. Törnevik, and A. Flodström, *Rev. Sci. Instrum.* **66**, 1398 (1995).

²⁰T. Munakata, T. Masuda, N. Ueno, S. Sakaya, T. Sugiyama, N. Takehiro, and Y. Sonoda, *Surf. Sci.* **532-535**, 1140 (2003).

²¹M. Källäne, K. Rossnagel, M. Marczynski-Bühlow, L. Kipp, H. I. Starnberg, and S. E. Stoltz, *Phys. Rev. Lett.* **100**, 065502 (2008).

²²X. J. Zhou, B. Wannberg, W. L. Yang, V. Brouet, Z. Sun, J. F. Douglas, D. Dessau, Z. Hussain, and Z.-X. Shen, *J. Electron Spectrosc. Relat. Phenom.* **142**, 27 (2005).

²³A. Pietzsch, A. Föhlisch, M. Beye, M. Deppe, F. Hennies, M. Nagasono, E. Suljoti, W. Wurth, C. Gahl, K. Döbrich, and A. Melnikov, *New J. Phys.* **10**, 033004 (2008).

²⁴S. Passlack, S. Mathias, O. Andreyev, D. Mittnacht, M. Aeschlimann, and M. Bauer, *J. Appl. Phys.* **100**, 024912 (2006).

²⁵J. P. Long, B. S. Itchkawitz, and M. N. Kabler, *J. Opt. Soc. Am. B* **13**, 201 (1996).

²⁶B. J. Siwick, J. R. Dwyer, R. E. Jordan, and R. J. D. Miller, *J. Appl. Phys.* **92**, 1643 (2002).

²⁷S. Hellmann, K. Rossnagel, M. Marczynski-Bühlow, and L. Kipp, *Phys. Rev. B* **79**, 035402 (2009).

²⁸J. Graf, S. Hellmann, C. Jozwiak, C. L. Smallwood, Z. Hussain, R. A. Kaindl, L. Kipp, K. Rossnagel, and A. Lanzara, *J. Appl. Phys.* **107**, 014912 (2010).

²⁹J. Barnes and P. Hut, *Nature (London)* **324**, 446 (1986).

³⁰T. Munakata and T. Kasuya, *Surf. Sci.* **283**, 452 (1993).

³¹G. Öhrwall, P. Karlsson, M. Wirde, M. Lundqvist, P. Andersson, D. Ceolin, B. Wannberg, T. Kachel, H. Dürr, W. Eberhardt, and S. Svensson, *J. Electron Spectrosc. Relat. Phenom.* **183**, 125 (2011).

³²A. Nambu, J.-M. Bussat, M. West, B. C. Sell, M. Watanabe, A. W. Kay, N. Mannella, B. A. Ludewigt, M. Press, B. Turko, G. Meddeler, G. Zizka, H. Spieler, H. van der Lippe, P. Denes, T. Ohta, Z. Hussain, and C. S. Fadley, *J. Electron Spectrosc. Relat. Phenom.* **137-140**, 691 (2004).